

Electrical conductivity in shaly sands with geophysical applications

A. Revil,¹ L. M. Cathles III, and S. Losh

Department of Geological Sciences, Global Basin Research Network Group, Cornell University, Ithaca, New York

J. A. Nunn

Department of Geology and Geophysics, Global Basin Research Network Group, Louisiana State University, Baton Rouge

Abstract. We develop a new electrical conductivity equation based on Bussian's model and accounting for the different behavior of ions in the pore space. The tortuosity of the transport of anions is independent of the salinity and corresponds to the bulk tortuosity of the pore space which is given by the product of the electrical formation factor F and the porosity ϕ . For the cations, the situation is different. At high salinities, the dominant paths for the electromigration of the cations are located in the interconnected pore space, and the tortuosity for the transport of cations is therefore the bulk tortuosity. As the salinity decreases, the dominant paths for transport of the cations shift from the pore space to the mineral water interface and consequently are subject to different tortuosities. This shift occurs at salinities corresponding to $\xi/t'_{(c)} \sim 1$, where ξ is the ratio between the surface conductivity of the grains and the electrolyte conductivity, and $t'_{(c)}$ is the Hittorf transport number for cations in the electrolyte. The electrical conductivity of granular porous media is determined as a function of pore fluid salinity, temperature, water and gas saturations, shale content, and porosity. The model provides a very good explanation for the variation of electrical conductivity with these parameters. Surface conduction at the mineral water interface is described with the Stern theory of the electrical double layer and is shown to be independent of the salinity in shaly sands above 10^{-3} mol L⁻¹. The model is applied to in situ salinity determination in the Gulf Coast, and it provides realistic salinity profiles in agreement with sampled pore water. The results clearly demonstrate the applicability of the equations to well log interpretation of shaly sands.

1. Introduction

Electrical conductivity can be used to infer porosity [Pezard, 1990], shale content, and gas or hydrocarbon saturation [Ellis, 1987]. However, interpretation is complicated by the presence of clay minerals. Clays consist essentially of alumino-silicate minerals, which have a deficit of charge due to (1) substitution of ions in the crystal structure by ions of different valence, and (2) acid/base reactions between surface silanol/aluminol groups and water [e.g., Thomas, 1976]. The "counterions" required to counterbalance this charge deficit are located in the so-called electrical double layer [Waxman and Smits, 1968; Avena and De Pauli, 1996; and Janusz et al., 1997]. The presence of these counterions shields the local electrical field produced by the charge deficit of the clay minerals and results in a macroscopic electrical static field equal to zero [Pride, 1994].

Under the influence of a macroscopic electrical field, as an applied electrical field or the result of charge separation in the bulk pore space due to a salinity gradient, the counterions

can move along the grains water surface [e.g., Zukoski and Saville, 1986; Revil and Glover, 1997]. The electrical conductivity of a saturated mixture of sand and clay grains is a combination of the bulk conductivity in the interconnected pore space and the surface conductivity at the grain water interface [Bussian, 1983]. Downhole electrical conductivity measurements are usually interpreted by empirical models such as the classical Waxman and Smits [1968] model, the dual-water model [Clavier et al., 1984], or variations of these models [e.g., Pezard, 1990]. In this paper we are interested in finding an improved relationship between the effective electrical conductivity of a shaly sand as a function of electrolyte conductivity, porosity, gas saturation, and clay properties.

A differential effective medium theory for the electrical conductivity of a saturated porous medium is used. Following Revil and Glover [1997], the model accounts for the different behavior of anions and cations. This model is applied to a mixture of sand grains and clay minerals. The surface electrical conductivity is controlled by the cation exchange capacity of the clay minerals. We apply our model to determine the salinity profiles in three boreholes in the South Eugene Island (SEI) Basin, offshore Louisiana, and discuss the salinity profiles derived.

¹Now at Laboratoire de Mesures en Forage, Aix-en-Provence, France.

Copyright 1998 by the American Geophysical Union.

Paper number 98JB02125.
0148-0227/98/98JB-02125 \$09.00

2. Model

We consider a granular porous medium with insulating grains saturated by a binary 1:1 electrolyte like NaCl. The

Table 1. Electrolytic (at Infinite Dilution) and Surface Ionic Mobilities, and Temperature Dependence of the Surface Mobilities for Some Possible Counterions at 25°C

Ion	β_p $10^{-8} \text{ m}^2 \text{ s}^{-1} \text{ V}^{-1}$	β_s $10^{-8} \text{ m}^2 \text{ s}^{-1} \text{ V}^{-1}$	ϑ_s $^{\circ}\text{C}^{-1}$
H ⁺	36.3	1.60 ^a	0.023 ^b
Li ⁺	4.00	0.50 ^a	0.094 ^c
Na ⁺	5.19	0.51 ^a	0.037 ^c
K ⁺	7.61	0.37 ^a	0.040 ^c
NH ₄ ⁺	7.60	0.23 ^a	-
Rb ⁺	8.06	0.20 ^a	-
Cs ⁺	8.00	0.15 ^a	0.049 ^c
Ba ²⁺	6.59	0.15 ^c	0.030 ^c
Ca ²⁺	6.16	0.13 ^a	0.040 ^c
Sr ²⁺	6.16	0.12 ^c	0.038 ^c
Mg ²⁺	5.48	0.10 ^a	0.040 ^c

^aFrom Raythatha and Sen [1986] on montmorillonite.

^bFrom Gast and East [1964] on a bentonite suspension.

^cFrom Hardwick [1987] on a shaly sandstone.

effect of gas content will be analyzed later in this paper. The Hanai-Bruggeman equation [Bruggeman, 1935; Hanai, 1960, 1961; Bussian, 1983] was developed using a self-consistent medium model of the dielectric and conductive responses of a composite in which charged insulating spheres of arbitrary size are suspended in a conducting fluid. Their approach is valid only in the limit $\phi \rightarrow 1$, where ϕ represents the fractional interconnected porosity. Sen et al. [1981] obtain the same analytical equation as Bruggeman [1935] and Hanai [1960] using a differential effective medium approach valid in all the porosity spectrum. In the model of Sen et al. [1981], spheres of non-conducting material, representing the insulating mineral grains, are added to a conducting fluid, which represents the saline water, until the desired porosity is reached. Their method assures that the fluid contains conducting pathways at all values of porosity. Bussian [1983] considered the insulating grains coated by a layer of surface conductivity Σ_S which represents the electrical conduction in the electrical double layer (diffuse and Stern layers).

In the present work, contrary to Bussian [1983] or de Lima and Sharma [1990], we explicitly include the different behavior of different charge carriers, that is, the anions and the cations. We specify $t_{(+)}^f$ and $t_{(-)}^f$ as the fraction of electrical current carried in the free electrolyte by the cations and the anions, respectively. These parameters are called the "Hittorf transport numbers" of the cations and anions in the free electrolyte [e.g., Revil and Glover, 1997] and $t_{(\pm)}^f = \beta_{(\pm)}^f / (\beta_{(+)}^f + \beta_{(-)}^f)$, where $\beta_{(\pm)}^f$ (in $\text{m}^2 \text{ s}^{-1} \text{ V}^{-1}$) are the ionic mobilities of the ions (Table 1). For NaCl, $t_{(+)}^f(\text{Na}^+) \approx 0.38$, and for KCl, $t_{(+)}^f(\text{K}^+) \approx 0.50$ [e.g., Thomas, 1976]. To first approximation, the Hittorf transport numbers in the free electrolyte are independent of both salinity and temperature [e.g., Thomas, 1976]. Similarly, we specify $t_{(+)}^s$ and $t_{(-)}^s$ as the fraction of current transported by cations and anions for surface conduction. These parameters are called the surface

Hittorf numbers of the cations and anions [Revil and Glover, 1997]. From the definitions of these parameters we have: $t_{(+)}^f + t_{(-)}^f = 1$ and $t_{(+)}^s + t_{(-)}^s = 1$.

The electrical conductivity of a granular porous medium is given by combining the definitions of the Hittorf transport number with the approach of Bussian [1983],

$$\sigma = \sigma_{(+)} + \sigma_{(-)}, \quad (1)$$

$$\sigma_{(\pm)} = t_{(\pm)}^f \sigma_f \phi^m \left(1 - \frac{t_{(\pm)}^s \sigma_s}{t_{(\pm)}^f \sigma_f} \right)^m \left(1 - \frac{t_{(\pm)}^s \sigma_s}{\sigma_{(\pm)}} \right)^{-m}. \quad (2)$$

Here $\sigma_{(\pm)}$ are the ionic contributions to the macroscopic electrical conductivity σ , σ_f is the pore fluid conductivity, m is called the "cementation exponent," $m = 3/2$ for perfect spherical grains [Sen et al., 1981], and ϕ is the interconnected fractional porosity of the sediment. The surface conductivity σ_s is related to the specific surface conductance Σ_S (in siemens) by $\sigma_s = 2\Sigma_S / R$ where R is the radius of the grains. This is because the effect of coating non-conducting grains with a specific surface conductivity Σ_S is exactly equivalent to increase the bulk conductivity by $2\Sigma_S / R$ [O'Konski, 1960]. The electrical formation factor F is defined by [Bussian, 1983]

$$\frac{1}{F} \equiv \lim_{\sigma_s \rightarrow 0} \left(\frac{\sigma}{\sigma_f} \right) = \phi^m. \quad (3)$$

Equation (3) represents the classical Archie's [1942] law. This law has been confirmed by numerical works [e.g., Roberts and Schwartz, 1985; Schwartz and Kimminau, 1987; Sen, 1987] which simulate electrical conduction in dense ordered or disordered packing of insulating spheres saturated by a conductive phase.

To obtain an analytical expression of (2), we use the approximation

$$\sigma_{(\pm)} \approx t_{(\pm)}^f \sigma_f \phi^m \left(1 - \frac{t_{(\pm)}^s \sigma_s}{t_{(\pm)}^f \sigma_f} \right)^2 \left(1 - \frac{t_{(\pm)}^s \sigma_s}{\sigma_{(\pm)}} \right)^{-2}, \quad (4)$$

which is formally exact for $m = 2$ and is a good approximation for $3/2 \leq m \leq 5/2$, the commonly observed range of cementation exponent in sedimentary rocks [e.g., Waxman and Smits, 1968]. Equation (4) can be rewritten as a second degree equation in $\sigma_{(\pm)}$, which can be easily solved. In the pH range 5-8, we can expect that the counterions of the electrical diffuse and Stern layers are mostly cations [e.g., Grosse and Foster, 1987; Avena and De Pauli, 1996; Revil and Glover, 1997], and therefore we consider $t_{(-)}^s = 0$. With this last assumption, (4) becomes

$$\sigma_{(+)} = \frac{\sigma_f}{F} \left[F\xi + \frac{1}{2} (t_{(+)}^f - \xi) \left(1 - \frac{\xi}{t_{(+)}^f} + \sqrt{\left(1 - \frac{\xi}{t_{(+)}^f} \right)^2 + \frac{4F\xi}{t_{(+)}^f}} \right) \right] \quad (5)$$

$$\sigma_{(-)} = \frac{1}{F} (1 - t_{(+)}^f) \sigma_f, \quad (6)$$

where ξ is a key dimensionless parameter defined by [Kan and Sen, 1987; Sen, 1987; Shubin et al., 1993]

$$\xi \equiv \frac{\sigma_s}{\sigma_f} = \frac{2\Sigma_S}{R\sigma_f} \approx \frac{2}{3} \frac{\phi}{1-\phi} \frac{Z_S \beta_S Q_V}{\sigma_f}. \quad (7)$$

Here β_S is an equivalent surface mobility for the surface electrical conduction process, Q_V is the excess of surface charge per unit pore volume (usually expressed in meq mL⁻¹, 1 meq mL⁻¹ = 96.32 x 10⁶ C m⁻³ in SI units where C represents Coulomb), and Z_S is the valence of the counterions (e.g., $Z_S = 1$ for Na⁺, Li⁺, and Cs⁺, $Z_S = 2$ for Ca²⁺). The parameter Q_V is related to the cation exchange capacity (CEC) by [e.g., Waxman and Smits, 1968]

$$Q_V \equiv \rho_g \frac{1-\phi}{\phi} \text{CEC.} \quad (8)$$

Here ρ_g is the grain density ($\approx 2650 \text{ kg m}^{-3}$ for quartz and clay minerals without their bound water).

The CEC (in meq g⁻¹ or C kg⁻¹ of matrix weight) indicates the maximum number of surface exchangeable cations per unit mass of sediment and is usually significant only for clay minerals [Ellis, 1987]. Patchett [1975] suggested a direct relationship between CEC and specific surface area (see Figure 1). The surface charge density is given by the ratio between the CEC and the specific surface area, which is equal to the ratio $Q_V/(S/V_p)$ where S is the surface area of the mineral water interface and V_p is the pore volume. The data of Figure 1 indicate a surface charge density of 1-3 elementary charges per nm² for all the clay minerals. Thomas [1976] gives the CEC for authigenic forms of the clay minerals: CEC(kaolinite) $\approx 0.03 \text{ meq g}^{-1}$, CEC(chlorite) $\approx 0.01 \text{ meq g}^{-1}$, CEC(illite) $\approx 0.09 \text{ meq g}^{-1}$ and CEC(smectite) $\approx 0.8 \text{ meq g}^{-1}$ [note: 1 meq g⁻¹ = ($e \mathcal{N}$) C kg⁻¹ = 96320 C kg⁻¹ where e is the elementary charge and \mathcal{N} is Avogadro's number]. The values given by Thomas are in agreement with the values given by Ridge [1983] and Ellis [1987]: CEC(kaolinite) ≈ 0.03 -0.15 meq g⁻¹, CEC(illite) ≈ 0.10 -0.40 meq g⁻¹, and CEC(Na-montmorillonite) ≈ 0.7 -0.8 meq g⁻¹ [Ridge, 1983], CEC(smectite) ≈ 0.8 -1.5 meq g⁻¹ [Ellis, 1987], and the values reported by Wiklander [1964]: CEC(kaolinite) $\approx 0.023 \text{ meq g}^{-1}$, CEC(illite) $\approx 0.16 \text{ meq g}^{-1}$ and CEC(Na-montmorillonite) $\approx 0.810 \text{ meq g}^{-1}$. For a mixture of clay minerals we can take an arithmetic average of individual clay CEC weighted by the corresponding volume fraction of each clay mineral to obtain the effective CEC [Pezard, 1990]. For a mixture of sand grains and clay minerals, the CEC can be calculated by [Patchett, 1975]

$$\text{CEC} = \phi_w \sum_i \chi_i \text{CEC}_i, \quad (9)$$

where CEC is the effective cation exchange capacity of the sediment, ϕ_w is the mass fraction of clay minerals in the sediment, χ_i are the relative fractions of each clay minerals in the shale fraction of the sediment, and CEC_i is the cation exchange capacity of each of these clay minerals. The cation exchange capacity corresponding to the quartz grains can be neglected due to the large size of these grains (and therefore the small amount of surface charge per unit mass) in comparison with the size of the clay minerals grains [Ellis, 1987].

Equations (5) and (6) assume that the tortuosity corresponding to the migration of the anions is given by $F\phi$, that is, the tortuosity of the interconnected pore space. For the cations the situation is different. At high salinities the dominant paths for the electro-migration of the cations are located in the interconnected pore space and the tortuosity for the transport of cations and anions is the same. As the salinity decreases, the dominant paths for the electro-

migration of the cations shift from the interconnected pore space to the grains water interface, and therefore are subject to different tortuosities [Sen, 1987]. This transition occurs at a salinity corresponding to $\xi/t_{(+)}^f \sim 1$, that is, $\sigma_f \sim \sigma_S / t_{(+)}^f$. The change is responsible for the curvature (the second partial derivative with respect to the electrolyte conductivity) of the electrical conductivity data of shaly sands when plotted as a function of the pore fluid conductivity at low salinities [e.g., Sen, 1987; Revil and Glover, 1997]. From (1), (5), and (6) we have

$$\sigma = \frac{\sigma_f}{F} \left[1 - t_{(+)}^f + F\xi + \frac{1}{2} (t_{(+)}^f - \xi) \times \left(1 - \frac{\xi}{t_{(+)}^f} + \sqrt{\left(1 - \frac{1}{t_{(+)}^f} \xi \right)^2 + \frac{4F}{t_{(+)}^f} \xi} \right) \right]. \quad (10)$$

The high-salinity asymptote of (10) corresponding to $\xi \ll 1$ is

$$\sigma = \frac{\sigma_f}{F} [1 + 2(F-1)\xi]. \quad (11)$$

We have tested (10) against experimental data (at 25°C, NaCl electrolyte) derived from databases of Hill and Milburn [1956], Waxman and Smits [1968], and Vinegar and Waxman [1984]. We have used all 129 samples from these databases with $0 \leq Q_V \leq 1.60 \text{ meq mL}^{-1}$ (1 meq mL⁻¹ = 96.32 x 10⁶ C m⁻³). From these electrical conductivity measurements we have solved (10) for F and ξ and estimate the surface electrical conductivity σ_S from (7) assuming that F is independent of the salinity because F is a microstructural parameter. The results are plotted in Figure 2, which shows that σ_S (and therefore Σ_S) is independent of the salinity. Possible explanations for surface electrical

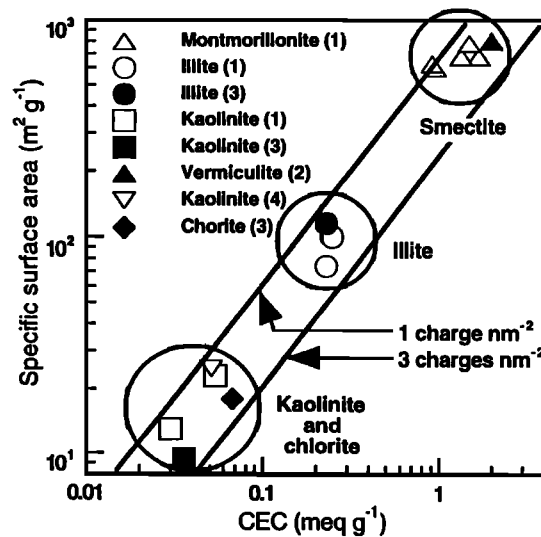


Figure 1. Variation of the specific surface area (in m² g⁻¹) with the CEC (in meq g⁻¹ with 1 meq g⁻¹ = 96320 C kg⁻¹) for various clay minerals. The ratio between the CEC and the specific surface area gives the equivalent surface charge density of the mineral surface Q_S . Experimental data are from 1, Patchett [1975]; 2, Lipsicas [1984]; 3, Zundel and Siffert [1985]; and 4, Lockhart [1980]. The grey areas represent the domains of variations for kaolinite and chlorite, illite, and smectite.

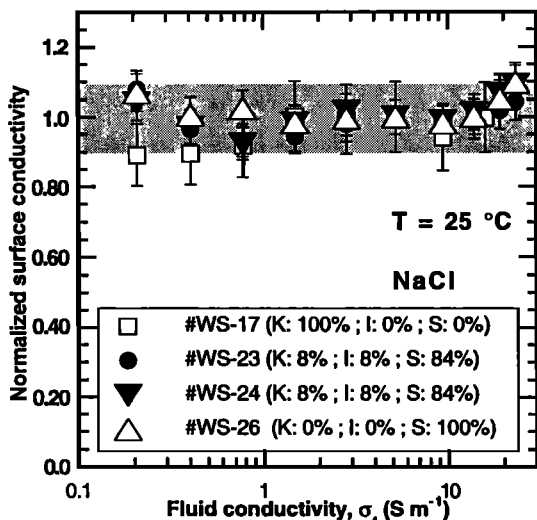


Figure 2. Normalized surface conductivity $\sigma_S(\sigma_f)/\sigma_S(5.249 \text{ S m}^{-1})$ as a function of the pore fluid conductivity σ_f . In the range of salinity investigated by Waxman and Smits [1968], the surface conductivity determined from the model described in the main text is constant inside a 10% variation by comparison with the value of the surface conductivity at $\sigma_f = 5.249 \text{ S m}^{-1}$ (shown by the grey band). The letters K, I, and S indicate kaolinite, illite, and smectite content respectively.

conductivity are conduction in the electrical diffuse layer [Revil and Glover, 1997], conduction in the Stern layer [Zukoski and Saville, 1986], and conduction at the mineral surface by proton transfer [O'Konski, 1960; S. Pride, personal communication, 1995]. Results plotted in Figure 2 are in contrast with electrical conduction in the electrical diffuse layer which is strongly salinity dependent [Revil and Glover, 1997]. We believe that surface electrical conduction in shaly sands is probably associated with electrical conduction in the Stern layer as postulated by Urban *et al.* [1935], Lorenz [1969] and Morimoto and Kittara [1973]. Zukoski and Saville [1986] have presented an electrokinetic model incorporating effects due to electromigration transport in the Stern layer. Shubin *et al.* [1993] came to similar conclusions regarding the role of surface conductivity in the Stern layer in their analysis of the frequency dependence of electrophoretic mobility of a monodisperse latex with carboxyl-head surface groups. Furthermore, Morimoto and Kittara [1973] and Hardwick [1987] have shown that surface conductivity is strongly dependent on brine composition. The experiments of Lorenz [1969] indicate that there is no surface conductivity at the isoelectric point of Na-kaolinite (at $\text{pH} \approx 4$). Both observations seem to exclude surface conduction by proton transfer as the main mechanism of surface conduction in shaly sands as it has been sometimes postulated.

In the Stern layer the counterions are directly adsorbed on the clay mineral surface through the surface coordination reactions [e.g., Avena and De Pauli, 1996; Janusz *et al.*, 1997],



Here the greater than sign represent the mineral lattice, Me represents Si or Al atoms, and $>\text{Si-O-Al}<$ (or SiAlO^-)

represents the groups arising from isomorphous substitutions of high-valence cations with those of lower valence in the tetrahedral framework of the clay minerals. Counterions can move along the pore surface probably by direct surface site interhopping. The net energy of interaction of the clay surface with the counterion may result from short-range chemical forces (covalent bonding, hydrophobic bonding, hydrogen bridges, steric or orientational effects) and long-range forces (electrostatic and van der Waals attraction forces), and the mobility of the counterions depends of the forces involved. The independence of surface conductivity for salinity above $10^{-3} \text{ mol L}^{-1}$ can be explained by the saturation of the Stern layer by Na^+ ions above this salinity at $\text{pH} = 7$ [e.g., Glover *et al.*, 1994, Figure 11]. At lower salt concentrations we would expect a decrease of the surface conductivity corresponding to a decrease of counterion adsorption in the Stern layer [Zukoski and Saville, 1986].

In this article we focus on the strictly dc-behavior of the electrical conductivity of shaly sands. In order to study the frequency-dependent response of a suspension of charged particles in an aqueous electrolyte, Grosse and Foster [1987] have replaced the double layer by a perfectly conducting layer for the cations and an insulating layer for the anions (both of zero thickness), and they include diffusion currents in the pore space. Because our results indicate that surface conduction is occurring mostly in the Stern layer, which has a thickness probably smaller than 10 \AA , the method used by Grosse and Foster [1987] could be combined with our results to derive the frequency behavior of the electrical conductivity of saturated shaly sands. This will be the purpose of a future work.

We assume from now that both the formation factor F and surface conductivity σ_S are independent of the salinity. We have calculated F and σ_S by fitting (10) nonlinearly to the

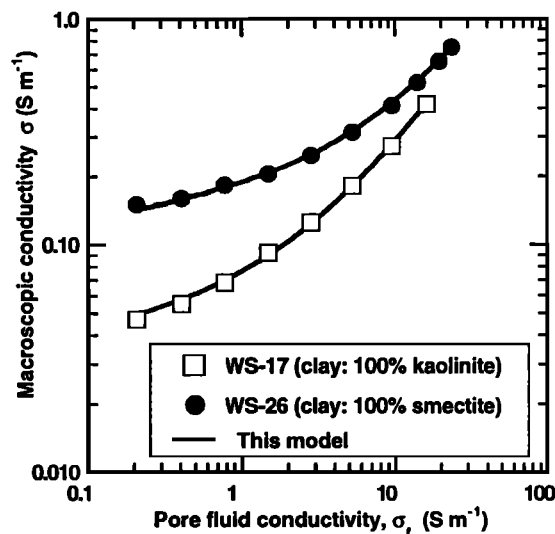


Figure 3. Macroscopic electrical conductivity σ as a function of pore fluid electrical conductivity σ_f . The equation developed in the main text, equation (10), is used to determine the electrical formation factor F and the surface conductivity σ_S (experimental data from Waxman and Smits, [1968]). The results of the nonlinear fit corresponding to the equation describing the macroscopic conductivity σ as a function of the pore fluid conductivity σ_f are #WS-17; $F = 46.48 \pm 0.42$, $\sigma_S = (426 \pm 11) \times 10^{-4} \text{ S m}^{-1}$; #WS-26; $F = 46.95 \pm 0.63$, $\sigma_S = (1521 \pm 29) \times 10^{-4} \text{ S m}^{-1}$.

experimental rock conductivity data as a function of fluid conductivity data for each of the 129 samples analyzed by Hill and Milburn [1956], Waxman and Smits [1968], and Vinegar and Waxman [1984]. Examples of such fit are given in Figure 3. A plot of $\sigma_s(1-\phi)/\phi$ as a function of Q_v for each of the 129 samples analyzed is given in Figure 4. The parameter Q_v is estimated from the CEC using (8), and the CEC is obtained from the chemical titration experiment of the clay fraction [Waxman and Smits, 1968]. A linear regression between $\sigma_s(1-\phi)/\phi$ and Q_v using (7) leads to the value of $\beta_s(25^\circ\text{C}) = 5.14 \times 10^{-9} \text{ m}^2 \text{ s}^{-1} \text{ V}^{-1}$ for the ion Na^+ in the Stern layer. Because the samples used in the previous databases have different proportions of kaolinite, smectite, and illite, β_s seems to be independent of the clay mineralogy. If we take a surface charge density Q_s ($= Q_v V_p / S$ where S is the surface area of the grains water interface and V_p is the pore volume) of three charges per nm^2 (Figure 1), the specific surface conductivity of clay minerals is $\Sigma_s(25^\circ\text{C}) = e Q_s \beta_s \approx 2.5 \times 10^{-9} \text{ S}$. This value is in agreement with other independent studies [e.g., Morimoto and Kittara, 1973; Patchett, 1975; Lorenz, 1969; Van der Put and Bijsterbosch, 1980; O'Brien and Rowlands, 1993; Shubin et al., 1993].

Using the electrical conductivity data of Raythatha and Sen [1986] and Hardwick [1987] and the present model of electrical conductivity, we have calculated the surface mobility β_s for counterions other than Na^+ (Table 1). The values reported in Table 1 are consistent with other determinations. For example, the ratio between the value obtained for Na^+ and Ca^{2+} is in agreement with the result of Lorenz [1969] in Na-kaolinite and Vinegar and Waxman [1984] in Na- and Ca-bentonite gels. According to these authors the mobility of Ca^{2+} ions multiply by the valence of Ca^{2+} represent 40% of the mobility of Na^+ ions in kaolinite. Zukoski and Saville [1986] reported $\beta_s(\text{H}^+) / \beta_f(\text{H}^+) \approx 0.05$ and $\beta_s(\text{K}^+) / \beta_f(\text{K}^+) \approx 0.05$ for a suspension of latex particles in HCl and KCl in agreement with the H^+ and K^+ values reported in Table 1. The values for the ratio between the surface mobility of Na^+ and the surface mobility of the ions Li^+ , K^+ , Cs^+ , and Ca^{2+} are also in very good agreement with the ratio values reported by Weiller and Chaussidon [1968] for montmorillonite at 25°C . We note

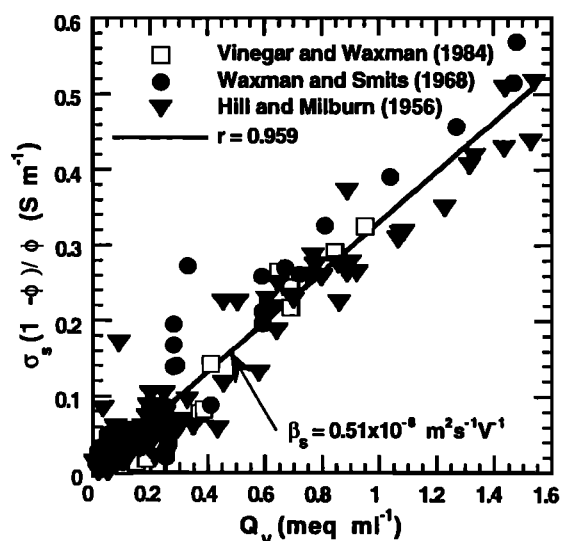


Figure 4. Surface conductivity σ_s as a function of excess charge density per unit pore volume Q_v .

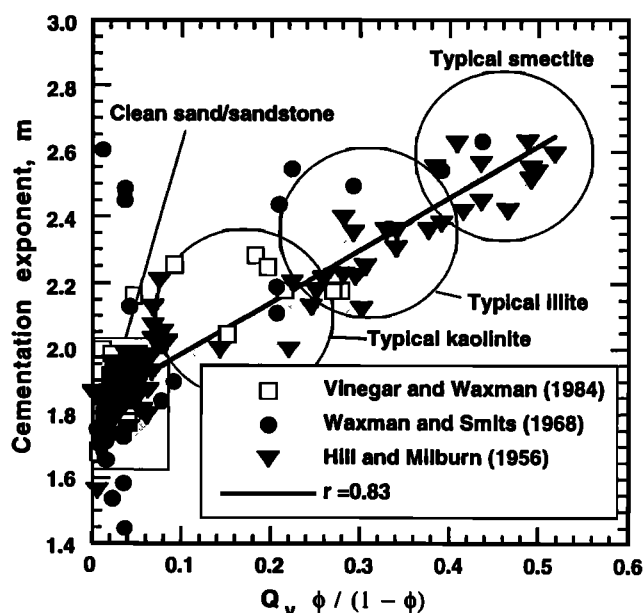


Figure 5. Cementation exponent in shaly sands. There is a net increase of the cementation exponent with the parameter $Q_v\phi/(1-\phi)$. The cementation exponent varies between 1.6-1.9 for clean sands and sandstones and 2.6 for smectite-rich sediments. The grey areas represent the domains of variation for clean sandstone, kaolinite, illite, and smectite.

that the mobilities of the counterions are given in a decreasing order according to the lyotropic serie: H^+ , $\text{Li}^+ \approx \text{Na}^+$, K^+ , NH_4^+ , Rb^+ , and Cs^+ . As noted by Vinegar and Waxman [1984] and Raythatha and Sen [1986], the binding between the clay minerals and the counterions in the Stern layer is determined primarily by Coulombic forces and decreases with increasing ionic radii and decreasing ionic charge. Vinegar and Waxman [1984] reported that the order of preference is generally $\text{Cs}^+ > \text{Rb}^+ > \text{K}^+ > \text{Na}^+ > \text{Li}^+$ for monovalent cations.

We have used the electrical conductivity databases discussed above in order to determine any variations between the cementation exponent m , which represents the decoupling factor between the total interconnected porosity and the effective porosity for the electrical current transport, and the factor $Q_v\phi/(1-\phi)$. We observe in Figure 5 a net increase of the cementation exponent with the factor $Q_v\phi/(1-\phi)$ which is directly proportional to the CEC as described by (8). Sandstones rich in smectite are observed to have the highest cementation exponent (Figure 5). For practical purposes, such dependence can be written by

$$m = m_0 + \alpha Q_v\phi/(1-\phi), \quad (13)$$

where m_0 represents the cementation exponent of a clean sand or sandstone (i.e., a sand or a sandstone without clay minerals, approximately $m_0 \approx 1.80$), and α is a coefficient relating the cementation exponent and CEC, $\alpha \approx 1.58 \text{ mL meq}^{-1}$.

Typically, the electrolyte and surface conductivities are temperature dependent. This dependence can be expressed with a linear form, which describes laboratory measurements very well (Figure 6),

$$\sigma_f(T) = \sigma_f(T_0) \left[1 + \vartheta_f(T - T_0) \right], \quad (14)$$

$$\beta_s(T) = \beta_s(T_0) \left[1 + \vartheta_s(T - T_0) \right], \quad (15)$$

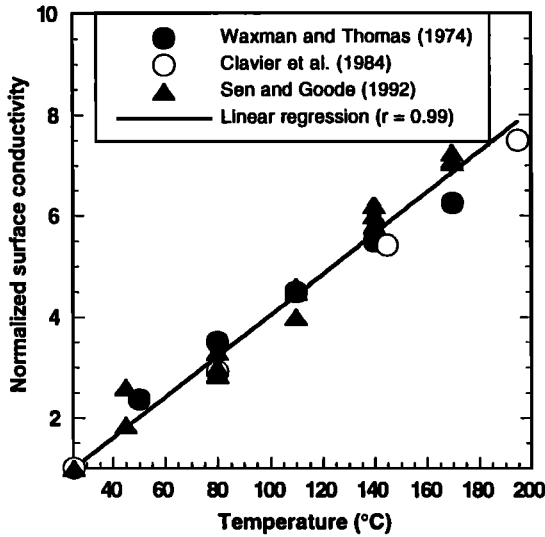


Figure 6. Normalized surface conductivity versus temperature. The surface conductivity of shaly sands at different temperatures and from various literature sources has been normalized to the surface conductivity at 25°C. A linear variation between these two parameters constitutes a very good approximation. The linear regression is forced through (25°C, 1).

where T_0 is a reference temperature (25°C), and the coefficients $\vartheta_f \approx 0.023 \text{ } ^\circ\text{C}^{-1}$, and $\vartheta_S(\text{Na}^+) \approx 0.040 \pm 0.002 \text{ } ^\circ\text{C}^{-1}$ (from Fig 6) are temperature independent. *Morimoto and Kittara* [1973] noted that the activation energy of surface conductivity of metal oxides is larger with larger adsorbed ions, and smaller with smaller adsorbed ions, compared to that of bulk conductivity. Using the electrical conductivity data on shaly sandstone of *Hardwick* [1987] and from *Gast and East* [1964] on a bentonite suspension and using the present model of electrical conductivity, we have calculated ϑ_S for counterions other than Na^+ (Table 1). Only two cations, Li and Cs, have values significantly higher than $0.040 \pm 0.002 \text{ } ^\circ\text{C}^{-1}$ in agreement with previous observations [e.g., *Gast and East*, 1964]. Because $\vartheta_S > \vartheta_f$, the ratio of the surface conductivity to the electrolyte conductivity increases with the temperature. At high temperatures, surface conductivity can dominate bulk conductivity even for high-salinity electrolytes in the pore space. For example, *Ward and Sill* [1983] reported a ratio of surface to water conductivity of ~ 3 for altered rocks at Roosevelt Hot Springs, Utah, despite the presence of an electrolyte containing 7000 ppm total dissolved solids (note: $1 \text{ ppm} = 58.443 \times 10^3 C_f / \rho_f$, where C_f is the equivalent NaCl solution concentration in mol L^{-1} and $58.443 \text{ g mol}^{-1}$ is the molecular mass of NaCl).

A case of great practical importance in hydrothermal areas and sedimentary basins is when two immiscible fluids occupy the pore space of a granular material. The particular case we develop here is that of two static fluids, only one conducts and is wetting for the mineral grains (the electrolyte) and the insulating fluid is nonwetting for the mineral grains (e.g., gas or oil). The influence of the nonwetting phase saturation upon the electrical conductivity can be taken into account by adding the transformation introduced by *Waxman and Smits* [1968] to the electrical conductivity equation, Eq. (10) [see *Waxman and Thomas*, 1974; *Clavier et al.*, 1984],

$$\phi^n \rightarrow \phi^n S_w^n, \quad (16a)$$

$$Q_V \rightarrow Q_V / S_w, \quad (16b)$$

where n is called the saturation or second Archie exponent ($n \approx m$) [*Waxman and Smits*, 1968; *Waxman and Thomas*, 1974; *Sen and Goode*, 1992] and S_w is the fractional water saturation of the pore space. A fully saturated pore space corresponds to $S_w = 1$. Values of the exponent n lie between 1.0 and 2.5 [*Dunlap et al.*, 1949]. In shaly sands, *Waxman and Thomas* [1974] give values of n typically in the range 1.6-2.2. Consequently the electrical conductivity as a function of the water saturation is given by

$$\sigma = \frac{\sigma_f S_w^n}{F} \left[1 - t_{(+)}^f + \frac{F\xi}{S_w^{n+1}} + \frac{1}{2} \left(t_{(+)}^f - \frac{\xi}{S_w} \right) \times \left(1 - \frac{\xi}{t_{(+)}^f S_w} + \sqrt{\left(1 - \frac{\xi}{t_{(+)}^f S_w} \right)^2 + \frac{4F\xi}{t_{(+)}^f S_w^{n+1}}} \right) \right]. \quad (17)$$

The presence of a nonwetting and insulating fluid phase (like gas or oil) in the interconnected pore space increases the ratio between surface to bulk properties.

3. Geophysical Application

Usually downhole measurement analysis of the electrical resistivity are done with the *Waxman and Smits* empirical model (WS-model) which has been the most widely accepted approach to the understanding of the electrical conductivity of shaly sands [e.g., *Ellis*, 1987]. The electrical conductivity in the WS model is given by [*Waxman and Smits*, 1968]

$$\sigma = \frac{1}{F} (\sigma_f + B Q_V), \quad (18)$$

where F is related to ϕ by the Archie relationship $F = \phi^{-2}$, and B is an equivalent counterion mobility given empirically at 25°C by

$$B = B_0 \left[1 - 0.6 \exp\left(-\frac{\sigma_f}{0.013}\right) \right], \quad (19)$$

where the electrolyte conductivity σ_f is in S m^{-1} and the maximum counterion mobility is given by $B_0 = 4.78 \times 10^{-8} \text{ m}^2 \text{ s}^{-1} \text{ V}^{-1}$. The form of (19) was chosen by *Waxman and Smits* [1968] to fit the curvature of the electrical conductivity data at low salinities. However, the decrease of the surface mobility with the salinity described by (19) is contrary to what could be expected from conventional physics. The curvature of σ when plotted as a function of the electrolyte conductivity is the result of the geometry of the porous medium as indicated by (19) (see also *Revil and Glover* [1997] and references therein, for a discussion of this effect based on Joule energy dissipation). As the salinity decreases, the dominant current paths shift from the pore volume to grain surfaces which have different tortuosities [e.g., *Sen and Goode*, 1992, and references therein]. Furthermore the scatter of B_0 -values can be significant ranging between $2 \times 10^{-8} \text{ m}^2 \text{ s}^{-1} \text{ V}^{-1}$ and $4.8 \times 10^{-8} \text{ m}^2 \text{ s}^{-1} \text{ V}^{-1}$. Predictions of our model are compared with predictions of the WS model in Figure 7. We use the high-salinity data (such that $\xi \ll 1$) of *Waxman and Smits* [1968], and we determine from our model and the WS model the electrical

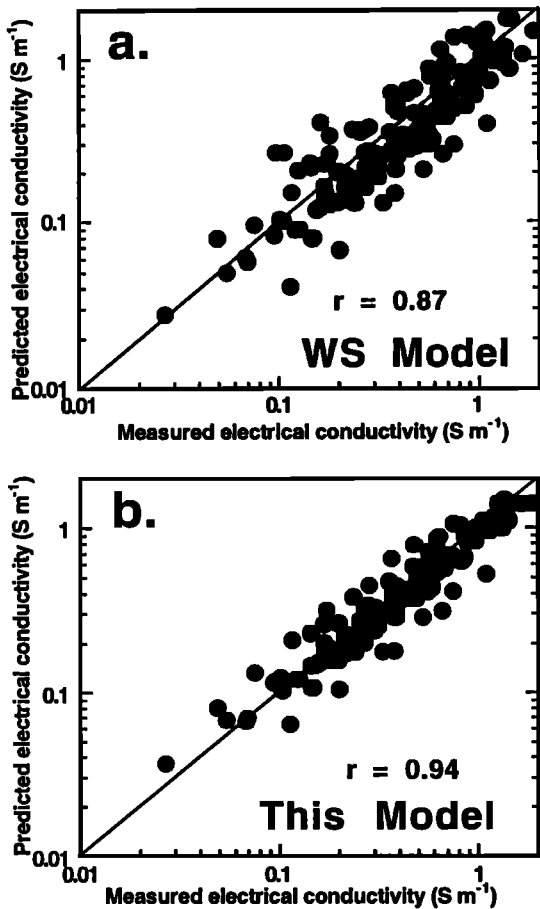


Figure 7. Predicted versus measured macroscopic electrical conductivity of shaly sands at 25°C (NaCl). The experimental data are from Waxman and Smits [1968]. Comparison between the model of Waxman and Smits [1968] and the model developed in this paper. The inputs are only the porosity and the chemical CEC.

conductivity from the porosity and the excess of counterions per unit pore volume. The results displayed in Figure 7 show that the model developed in this paper leads to an improvement in the ability to predict laboratory electrical conductivity measurements.

We apply the electrical conductivity model developed in this paper to determine salinity profiles in the South Eugene Island (SEI) salt withdrawal minibasin. This minibasin is a young Pleistocene passive shelfmargin sedimentary basin located in the Gulf of Mexico offshore Louisiana (Figure 8).

This basin was filled rapidly (sedimentation rate ~2 km/m.y.) over the last 2.8 Ma. During this period, a thick sequence of shale was deposited over pre-Tertiary sediments and covered by increasingly sand-rich sediments [Holland et al., 1990; Alexander and Flemings, 1995]. Below 1-2 km the pore fluid pressure is usually in excess of hydrostatic pressure [Holland et al., 1990]. The SEI area is crossed by some important faults and pierced by salt domes.

The natural gamma ray tool contains a gamma detector measuring the gamma quanta emitted by the decay of naturally occurring radioactive nuclei (potassium, thorium, uranium isotopes and their daughter nuclei) in the formations. Consequently, the gamma ray log is a measure of the natural radioactivity of the sediment formations and can be used to estimate the shaliness of the formations [Ellis, 1987]. We assume that the gamma ray is a linear function of the clay content,

$$\gamma = (1 - \phi_w)\gamma_{sd} + \phi_w\gamma_{sh}, \tag{20}$$

where γ is the gamma ray reading, γ_{sd} is the gamma ray of a pure sand assumed to be equal to 10 gamma ray units, whereas γ_{sh} is the gamma ray of a pure shale. The gamma ray level of a pure shale is calculated by:

$$\gamma_{sh} = \sum_{i=1}^n \chi_i \gamma_i, \tag{21}$$

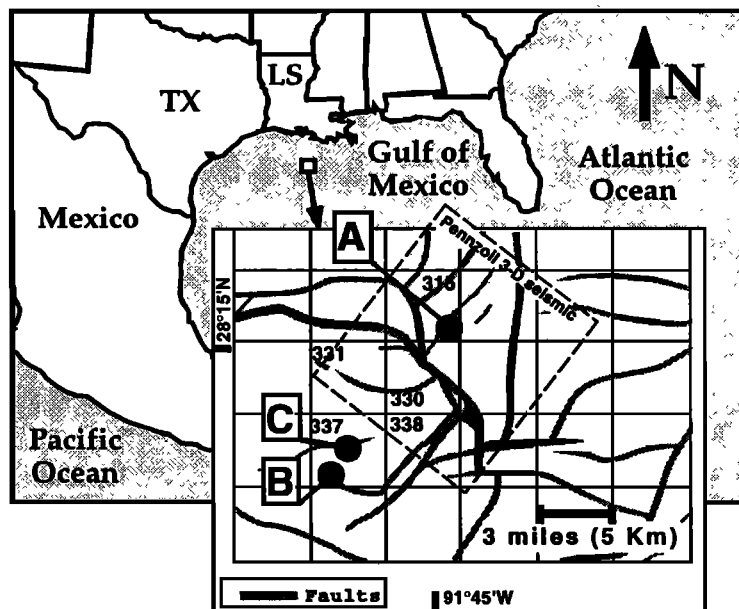


Figure 8. Location map of South Eugene Island (SEI) area. The SEI area is located on the continental shelf of offshore Louisiana. The sedimentation rate has been high since the Pleistocene (approximately 1.5-2.5 km/m.y.), and salt diapirism is intense in this area. The network of faults is interpreted from seismic data at a depth of 2 km. A, B, and C are well locations.

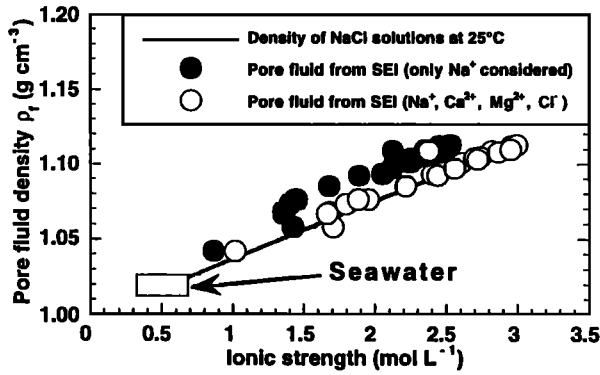


Figure 9. Pore fluid density as a function of the ionic strength of the pore water samples from the SEI area. Experimental data from pore water extracted from SEI cores are compared with data for pure NaCl electrolyte. They are both in agreement if we consider the ionic strength at the place of the salinity of an equivalent NaCl solution. The ionic strengths derived from pore water sampled in the SEI area is in the range 0.5-3 mol L⁻¹.

where χ_i are the clay ratio of each clay mineral to the total shale fraction, and γ_i is the gamma ray level for each clay mineral. In the case considered in this paper, the clay mineralogy does not change all along the entire well sections. Thin sections we have analyzed indicate that the relative clay fractions in the sediment are fairly constant over the depth intervals selected. The clay ratios are approximately $\chi(I) = 1.75\%$; $\chi(C) = 18.25\%$; $\chi(MLC) = 64.5\%$ (with 25% of illite and 75% of smectite), and $\chi(K) = 15.5\%$ where I, C, MLC, and K represents illite, chlorite, mixed layers clays, and kaolinite respectively. The gamma ray levels for pure shale are $\gamma(I) \approx 250$; $\gamma(C) \approx 180$; $\gamma(MLC) \approx 100$; and $\gamma(K) \approx 80$ [Ellis, 1987]. With the previous values for the clay mineralogy and the gamma ray level for each component, we calculate from (21) $\gamma_{Sh} \approx 115$. From Eq. (20), the clay weight fraction of the formations is given by:

$$\phi_w = \frac{\gamma - \gamma_{sd}}{\gamma_{sh} - \gamma_{sd}}. \quad (22)$$

Equation (22) should be considered as a rough approximation because sometimes nonradioactive clay minerals are present and because uranium rich formations can be interpreted as shale layers [Ellis, 1987]. From (9), the clay composition previously described and the authigenic clay CEC data of Thomas [1976] we obtain $CEC \approx (0.0793 \phi_w) \text{ meq g}^{-1}$. This leads to a very good agreement with the values given by Clavier *et al.* [1984, their Fig. 1], who noted a direct correlation between (γ / ϕ) and Q_v : $Q_v \approx 1.2186 \times 10^{-3} (\gamma / \phi)$ for shaly sand.

The ionic strength I of a multicomponent electrolyte is defined by $I = \sum_{i=1}^n (Z_i)^2 C_i^f$ [e.g., Revil and Glover, 1997]. Here Z_i are the ionic valences, n is the number of ionic species and C_i^f are the ionic concentrations (in mol L⁻¹). The four main ions in the fluid sampled in the SEI area are Cl⁻, Na⁺, Ca²⁺, and Mg²⁺. Figure 9 shows that the sampled pore fluid in the SEI area is a multi-component electrolyte. It can be considered as an equivalent NaCl solution if we consider the salinity as equal to the ionic strength of the pore fluid taking into account the concentrations of the four main

ions Cl⁻, Na⁺, Ca²⁺, and Mg²⁺. The pore fluids sampled in the SEI area show very high salinities with ionic strength in the range 1-3 mol L⁻¹ (Figure 9), and fluid densities in the range 1040-1110 kg m⁻³ with an average value close to 1092 kg m⁻³ (Figure 9). For such salinities and the previous composition of the shale fraction, (7) gives $\xi \ll 1$, and therefore (11) can be used to infer salinity from electrical conductivity.

The result from the analysis of three wells is shown in Figure 10 (for borehole locations, see Figure 8). For this analysis we have used the electrical resistivity, the gamma ray, and the density logs, and the following methodology. The porosity is determined directly from the density log using the relationship $\rho = (1 - \phi)\rho_g + \phi\rho_f$ where ρ_f is the pore fluid density ($\approx 1092 \text{ kg m}^{-3}$, as seen previously). Consequently, the porosity is given by

$$\phi = \frac{\rho_g - \rho}{\rho_g - \rho_f}. \quad (23)$$

The porosity of the sediments in sedimentary basins decreases in a regular fashion as effective stress increases. A. Revil and L.M. Cathles (manuscript in preparation, 1998) show that the relationship between the hydrostatic porosity ϕ_H (the porosity corresponding to hydrostatic pore fluid pressure) and the depth of burial z is

$$\phi_H(z) = 1 - (1 - \phi_0) \exp\left(\frac{z}{z_c}\right), \quad (24)$$

where ϕ_0 is a noncompacted porosity, and z_c is a characteristic depth defined by $1/z_c \equiv \phi_0(\rho_g - \rho_f)g\beta$, ρ_g is the grain density, ρ_f is the density of the pore fluid, g is the acceleration of gravity, and β is a long-term porosity compressibility. This long-term compressibility is defined by $\beta \equiv -(1/\phi_0)(d\phi/d\sigma_{eff})$, where $\sigma_{eff} = \sigma - p \approx P - p$ is the effective stress, σ is the total confining pressure (i.e., the first total stress invariant), P is the lithostatic stress, and p is the total fluid pressure. Both ϕ_0 and β can be deduced from the porosity trend in the upper hydrostatic compartments (compartments A) shown in Figure 10.

Disequilibrium compaction occurs when sediments are unable to expel their pore fluid in response to sediment loading and fluid overpressures are generated. In such a case, the porosity remains a function of the effective stress [e.g., Bredehoeft and Hanshaw, 1968]. The total fluid pressure p is equal to the hydrostatic fluid pressure p_H plus the fluid overpressure δp . If the porosity ϕ is written as

$$\phi(z) = \phi_H(z) + \delta\phi(z), \quad (25)$$

A. Revil and L. M. Cathles (manuscript in preparation, 1998) show that the "excess porosity" $\delta\phi$ is related exactly to the excess fluid pressure δp by

$$\delta p(z) = \frac{\delta\phi(z)}{\phi_0\beta} - \int_0^z (\rho_g - \rho_f)g\delta\phi(z') dz'. \quad (26)$$

The second term corrects the lithostatic pressure for changes in sediment density due to the porosity change $\delta\phi$. Equation (26) is valid only for disequilibrium compaction. The excess porosity is indicated by the cross-hatched zones in Figure 10. The fluid overpressures determined from (26) are favorably compared to mud weight data which are known to be fairly

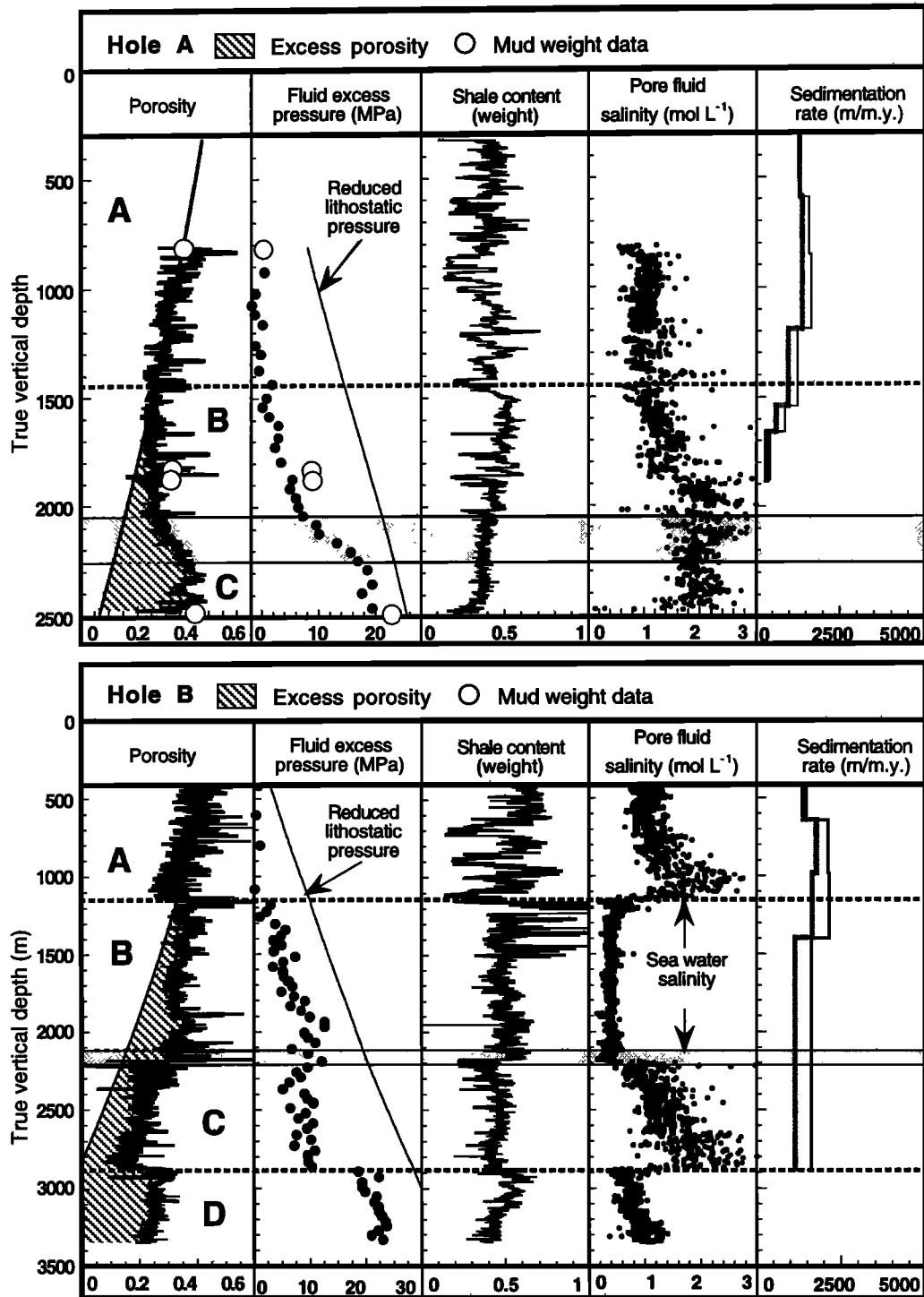


Figure 10. Results from the downhole measurements analysis. Porosity, fluid excess pressure (in megapascals), shale content (fractional weight with values between 0, clean sand, and 1, pure shale), pore fluid salinity (in mol L⁻¹), and sedimentation rate are derived from downhole measurements. The porosity and the shale content are derived from the density log and the gamma ray log, respectively. The porosity decreases almost linearly with the depth of burial in the upper hydrostatically pressured compartment (compartment A). Such decrease is characteristic of equilibrium compaction. The porosity trend in this compartment is indicated by the solid (almost linear) line. Fluid overpressure is computed from the excess porosity distribution (cross-hatched zone) defined by the difference between the porosity computed from the density log and the porosity predicted from the equilibrium compaction trend. Overpressured compartments are indicated by capital letters (B, C, and D). Dashed lines and shaded zones represent the boundaries between these compartments which correspond to the presence of seals or growing faults. The sedimentation rate is determined from biostratigraphic information (the lower value corresponds to the compacted sedimentation rate, and the higher value corresponds to the uncompacted sedimentation rate, see main text). The salinity is computed from the electrical conductivity equations derived in the main text, the electrical resistivity log, the porosity, and the shale content.

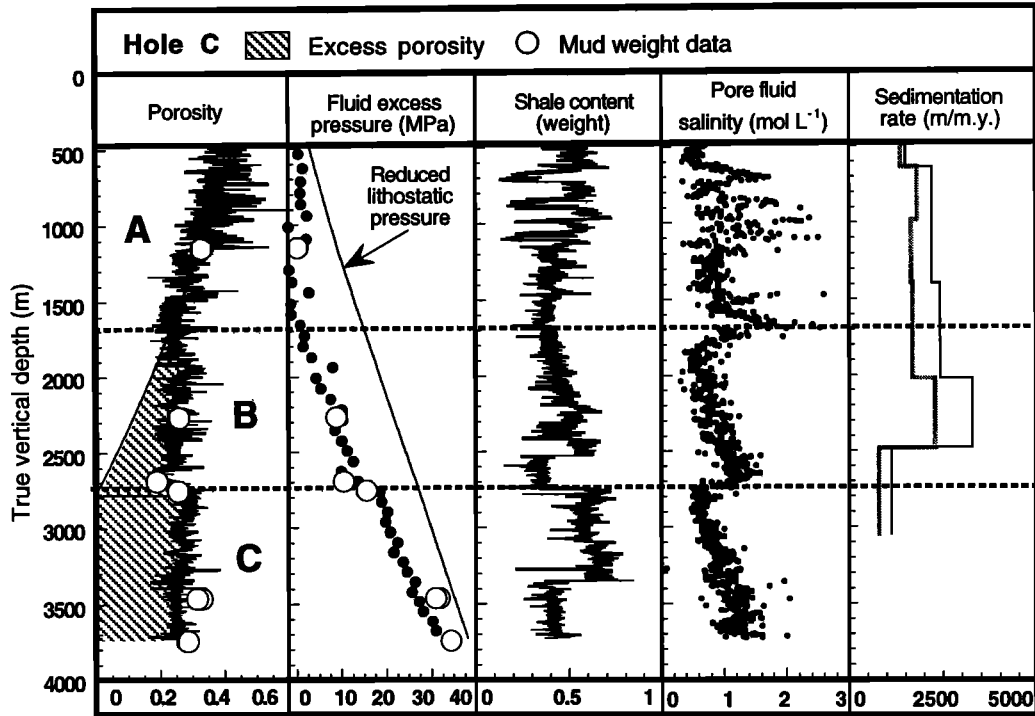


Figure 10. (continued)

good indicators of excess fluid pressures [Ellis, 1987]. The compacted sedimentation rate is equal to the thickness of the stratigraphic intervals divided by the time required for deposition. We estimate its magnitude from biostratigraphic information. This sedimentation rate ω is corrected from compaction to obtain a non-compacted sedimentation rate ω_0 using: $\omega_0 = \omega(1-\phi)/(1-\phi_0)$, where ϕ is determined from (23) and ϕ_0 from the normal trend of compaction.

The salinity is obtained from the set of equations given in the previous section of this paper using the following steps. (1) The CEC is obtained from (9), the shale content (in weight) obtained from (22) using the gamma ray log and the relative fractions of clay minerals. The CEC is converted to Q_V using (8). (2) The surface conductivity is calculated from (7) and corrected for temperature using (15). (3) The fluid conductivity is determined using (11) and corrected for temperature using (14) to obtain the pore fluid conductivity at 25°C. Integration of downhole temperature measurements (corrected from borehole effects) show that the variation of the temperature (in °C) with depth in the area is given by $T = T_S + G z_{\text{TVD}}$, where $T_S \approx 25^\circ\text{C}$ is the seafloor temperature, $G = 20.7 \times 10^{-3} \text{ }^\circ\text{C m}^{-1}$ is the large-scale geothermal gradient, and z_{TVD} is the true vertical depth below the seafloor. (4) Finally, because the salinity is roughly proportional to the electrolyte conductivity, we can estimate the salinity using $C_f \approx 0.56 \times [\sigma_f(25^\circ\text{C})/5]$, where 5 S m^{-1} is approximately the seawater electrical conductivity at 25°C and 0.56 mol L^{-1} is the salinity of an equivalent NaCl solution of same electrical conductivity than sea water according to the equation developed by Sen and Goode [1992].

Figure 10 shows porosity, fluid overpressure, sedimentation rate, and salinity profiles determined from the previous methodology. This suggests that the SEI basin is pressure compartmentalized maybe as a result of capillary

sealing [Revil et al., 1998]. Compartments are indicated by capital letters in Figure 10 (A, B, C, and D where A is always an hydrostatic compartment). The correlation of porosity and salinity variations suggests that porosity and salinity may have a common history. We note that the porosity variations and the salinity variations have roughly the same amplitude (approximately a factor 3) which could indicate the possible filtration effect of shale [Hanshaw and Copley, 1973]. However, salinity in the SEI area can also be controlled by salt dissolution of allochthonous salt structures and thermohaline convection [e.g., Hanor, 1987]. Salt domes pierce sedimentary layers and exist at shallow depth in the SEI area [Holland et al., 1990]. Preferential dissolution of the salt is occurring near the top of the dome [e.g., Hanor, 1987]. Less saline water bleeds up around salt domes where less saline overpressured fluids leak up from below resulting in gravitational instabilities and thermohaline convection. Regardless of the cause, the salinity pattern determined by the present method is remarkably coherent. Numerical modeling and theoretical analysis to explain the salinity, porosity, and pressure pattern will be addressed in a future paper.

4. Conclusions

We have developed a new model for the electrical conductivity of shaly sands which includes the influence of clay minerals (clay content and clay composition), ionic composition in the pore water and in the electrical double layer, temperature, and gas saturation. Ion transport along the surface of clay minerals occurs mainly in the Stern layer, where at 25°C, ion mobilities are smaller than in the bulk water. The temperature dependence of surface conductivity is generally higher than the temperature dependence of the bulk electrolyte. Consequently, surface conductivity can

represent an important contribution to the macroscopic conductivity of shaly sands in sedimentary basins and geothermal areas due to the increase of temperature with depth. At constant temperature the surface conductivity is shown to be independent of the salinity, at least for salinity above 10^{-3} mol L⁻¹. Electrical conductivity calculated with this model is favorably compared with published experimental data. We find consistent results of the electrical conductivity for shaly sands over a wide range of salinity, porosity, cation exchange capacity, and temperature. The application of this model in a sedimentary basin in the Gulf Coast of Mexico (South Eugene Island, offshore Louisiana) shows salinity profiles which are consistent with sampled salinity and indicating compartmentation of this basin.

Acknowledgments. This work is supported by the Gas Research Institute given number 5093-260-2689, the Global Basin Research Network (GBRN) at Cornell University, and the companies sponsoring these projects. This work benefited greatly from discussions with Y. Bernabé and P. A. Pezard and initially with M. Darot at Strasbourg. A. Revil acknowledges the support of Elf Aquitaine, O. Brevart, and D. Grauls during his stay at Cornell University. We thank D. Fitterman, P. Glover, and the associate editor G. Jiracek for their helpful reviews.

References

- Alexander, L. L., and P. B. Flemings, Geologic evolution of a Pliocene-Pleistocene salt withdrawal mini-basin: Eugene Island Block 330, offshore Louisiana, *AAPG Bull.*, **79**, 1737-1756, 1995.
- Archie, G. E., The electrical resistivity log as an aid in determining some reservoir characteristics, *Trans. Am. Inst. Min. Metall. Pet. Eng.*, **146**, 54-62, 1942.
- Avena, M. J., and C. P. De Pauli, Modeling the interfacial properties of an amorphous aluminosilicate dispersed in aqueous NaCl solutions, *Colloids Surf.*, **118**, 75-87, 1996.
- Bredehoeft, J. D., and B. B. Hanshaw, On the maintenance of anomalous fluid pressures in thick sedimentary sequences, *Geol. Soc. Am. Bull.*, **79**, 1097-1106, 1968.
- Bruggeman, D. A. G., Berechnung verschiedener physikalischer konstanten von heterogenen substanzen, *Ann. Phys.*, **24**, 636-664, 1935.
- Bussian, A. E., Electrical conductance in a porous medium, *Geophysics*, **48**, 1258-1268, 1983.
- Clavier, C., G. Coates, and J. Dumanoir, The theoretical and experimental bases for the dual-water model for the interpretation of shaly sands, *Soc. Pet. Eng. J.*, **24**(2), 153-169, 1984.
- de Lima, O. A. L., and M. M. Sharma, A grain conductivity approach to shaly sandstones, *Geophysics*, **55**, 1347-1356, 1990.
- Dunlap, H. F., H. L. Bilhartz, E. Schuler, and C. R. Bailey, The relation between electrical resistivity and brine saturation in reservoir rocks, *Trans. Am. Inst. Min. Metall. Pet. Eng.*, **186**, 259-264, 1949.
- Ellis, D. V., *Well Logging for Earth Scientists*, 527 pp., Elsevier, New York, 1987.
- Gast, R. G., and P. J. East, Potentiometric, electrical conductance and self-diffusion measurements in clay-water systems, *Clays Clay Miner.*, **12**, 297-310, 1964.
- Glover, P. W. J., P. G. Meredith, P. R. Sammonds, and A. F. Murrell, Ionic surface electrical conductivity in sandstone, *J. Geophys. Res.*, **99**, 21635-21650, 1994.
- Grosse, C., and K. R. Foster, Permittivity of a suspension of charged spherical particles in electrolyte solution, *J. Chem. Phys.*, **91**, 3073-3076, 1987.
- Hanai, T., Theory of the dielectric dispersion due to the interfacial polarization and its application to emulsions, *Kolloid-Z.*, **171**, 23-31, 1960.
- Hanai, T., Dielectric on the interfacial polarization for two-phase mixtures, *Bull. Inst. Chem. Res., Kyoto Univ.*, **39**, 341-367, 1961.
- Hanor, J. S., Kilometer-scale thermohaline overturn of pore waters in the Louisiana Gulf Coast, *Nature*, **327**, 501-503, 1987.
- Hanshaw, B. B., and T. B. Coplen, Ultrafiltration by a compacted clay membrane - II. Sodium ion exclusion at various ionic strengths, *Geochim. Cosmochim. Acta*, **37**, 2311-2327, 1973.
- Hardwick, A., The effect of brine composition on excess conductivity in shaly sands, paper presented at SPWLA 28th Annual Logging Symposium, Soc. of Prof. Well Log Anal., London, England, June 29-July 2, Paper VV, 1987.
- Hill, H. J., and J. D. Milburn, Effect of clay and water salinity on electrochemical behavior of reservoir rocks, *Trans., Am. Inst. Min. Metall. Pet. Eng.*, **207**, 65-72, 1956.
- Holland, D. S., J. B. Leedy, and D. R. Lammelin, Eugene Island Block 330 field - USA, offshore Louisiana, in *Compilers, Structural Traps; III, Tectonic Fold and Fault Traps, Treatise of Petroleum Geology Atlas of Oil and Gas Fields*, edited by E. A. Beaumont, and N. H. Foster pp. 103-143, Am. Assoc. of Pet. Geol., Tulsa, Okla., 1990.
- Janusz, W., I. Kobal, A. Sworska, and J. Szczypa, Investigation of the electrical double layer in a metal oxide/monovalent electrolyte solution system, *J. Colloid Interface Sci.*, **187**, 381-387, 1997.
- Kan, R., and P. N. Sen, Electrolytic conduction in periodic arrays of insulators with charges, *J. Chem. Phys.*, **86**, 5748-5756, 1987.
- Lipsicas, M., Molecular and surface interactions in clay intercalates, in *Physics and Chemistry of porous Media*, edited by D. L. Johnson and P. N. Sen, pp. 191-202, Am. Inst. of Phys., New York, 1984.
- Lockhart, N. C., Electrical properties and the surface characteristics and structure of clays, II, Kaolinite: A nonswelling clay, *J. Colloid Interface Sci.*, **74**, 520-529, 1980.
- Lorenz, P. B., Surface conductance and electrokinetic properties of kaolinite beds, *Clays Clay Miner.*, **17**, 223-231, 1969.
- Morimoto, T., and S. Kittara, Surface conductance of metal oxides in electrolyte solutions, *J. Colloid Interface Sci.*, **44**, 289-297, 1973.
- O'Brien, R. W., and W. N. Rowlands, Measuring the surface conductance of kaolinite particles, *J. Colloid Interface Sci.*, **159**, 471-476, 1993.
- O'Konski, C. T., Electric properties of macromolecules, V, Theory of ionic polarization in polyelectrolytes, *J. Chem. Phys.*, **64**, 605-619, 1960.
- Patchett, J. G., An investigation of shale conductivity, paper presented at SPWLA 16th Annual Logging Symposium, Soc. of Prof. Well Log Anal., Paper V, 40 pp., New Orleans, June 4-7, 1975.
- Pezard, P. A., Electrical properties of mid-ocean ridge basalt and implications for the structure of the oceanic crust in Hole 504B, *J. Geophys. Res.*, **95**, 9237-9264, 1990.
- Pride, S., Governing equations for the coupled electromagnetics and acoustics of porous media, *Phys. Rev. B*, **50**, 15678-15696, 1994.
- Raythatha, R., and P. N. Sen, Dielectric properties of clay suspensions in MHz to GHz range, *J. Colloid Interface Sci.*, **109**, 301-309, 1986.
- Revil, A., L. M. Cathles III, J. D. Shosa, P. A. Pezard, and F. D. de Larouzière, Capillary sealing in sedimentary basins: A clear field example, *Geophys. Res. Lett.*, **25**, 389-392, 1998.
- Revil, A., and P. W. J. Glover, Theory of ionic surface electrical conduction in porous media, *Phys. Rev. B*, **55**, 1757-1773, 1997.
- Ridge, M. J., A combustion method to measure the cation exchange capacity of clay minerals, *Log Anal.*, **3**, 6-11, 1983.
- Roberts, J. N., and L. M. Schwartz, Grain consolidation and electrical conductivity in porous media, *Phys. Rev. B*, **31**, 5990-5997, 1985.
- Sen, P. N., Electrolytic conduction past arrays of charged insulating spheres, *J. Chem. Phys.*, **87**(7), 4100-4107, 1987.
- Sen, P. N., and P. A. Goode, Influence of temperature on electrical conductivity on shaly sands, *Geophysics*, **57**, 89-96, 1992.
- Sen, P. N., C. Scala, and M. H. Cohen, Self similar model for sedimentary rocks with application to the dielectric constant of fused glass beads, *Geophysics*, **46**, 781-795, 1981.
- Schwartz, L. M., and S. Kimmjau, Analysis of electrical conduction in the grain consolidation model, *Geophysics*, **52**, 1402-1411, 1987.

- Shubin, V. E., R. J. Hunter, and R. W. O'Brien, Electroacoustic and dielectric study of surface conduction, *J. Colloid Interface Sci.*, *159*, 174-183, 1993.
- Thomas, E. C., Determination of Q_v from membrane potential measurements on shaly sands, *Trans. Am. Inst. Min. Metall. Pet. Eng.*, *261*, 1087-1096, 1976.
- Urban, F., H. L. White, and E. A. Stassner, Contribution to the theory of surface conductivity at solid-liquid interfaces, *J. Phys. Chem.*, *39*, 311-330, 1935.
- Van der Put, A. G., and B. H. Bijsterbosch, Electrical conductivity of dilute and concentrated aqueous dispersions of monodisperse polystyrene particles: Influence of surface conductance and double-layer polarization, *J. Colloid Interface Sci.*, *75*, 512-523, 1980.
- Vinegar, H. J., and M. H. Waxman, Induced polarization of shaly sands. The effect of clay counterion type, paper presented at SPWLA, Soc. of Prof. Well Log Anal., 1984.
- Ward, S. H., and W. R. Sill, Resistivity, induced polarization, and self-potential methods in geothermal exploration, *Rep. 1983-3*, Geothermal Training Programme, United Nations Univ., Reykjavik, Iceland, 1983.
- Waxman, M. H. and L. J. M. Smits, Electrical conductivities in oil-bearing shaly sands, *Soc. Pet. Eng. J.*, *8*, 107-122, 1968.
- Waxman, M. H., and E. C. Thomas, Electrical conductivities in shaly sands, *J. Pet. Technol.*, *257*, 213-225, 1974.
- Weiller, R. A., and J. Chaussidon, Surface conductivity and dielectrical properties of Montmorillonite gels, *Clays Clay Miner.*, *16*, 147-155, 1968.
- Wiklander, L., *Chemistry of the Soil*, 2nd ed., edited by F. E. Bear, Van Nostrand Reinhold, New York, 1964.
- Zukoski, C. F., and D. A. Saville, The interpretation of electrokinetic measurements using a dynamic model of the Stern layer, I, The dynamic model, *J. Colloid Interface Sci.*, *114*, 32-44, 1986.
- Zundel, J. P. and B. Siffert, Mécanisme de rétention de l'octylbenzene sulfonate de sodium sur les minéraux argileux, in *Solid-Liquid Interactions in Porous Media*, pp. 447-462, Technip, Paris, 1985.

L. M. Cathles III and S. Losh, Department of Geological Sciences, Snee Hall, Cornell University, GBRN Group, Ithaca, NY 14853. (e-mail: cathles@geology.cornell.edu; losh@geology.cornell.edu)

J.A. Nunn, Department of Geology and Geophysics, Louisiana State University, GBRN Group, Baton Rouge, LA 70803. (e-mail: jeff@geol.lsu.edu)

A. Revil, Laboratoire de Mesures en Forage, ODP, BP 72, 13545 Aix-en-Provence, Cedex 4, France. (e-mail: revil@lmf-aix.gulliver.fr)

(Received September 5, 1997; revised March 3, 1998; accepted June 15, 1998.)